Final Project Report

(Project# DE-SC0008312)

Collaborative Research: Fundamental studies of plasma control using surface embedded electronic devices

Principal Investigator: Laxminarayan L Raja
Department of Aerospace Engineering and Engineering Mechanics
The University of Texas at Austin

To: Nirmal Podder (Program Manager)
Office of Fusion Energy Sciences
U.S. Department of Energy

December 2015

Summary of Key Accomplishments:

We start with a listing of key accomplishments made as part of this NSF/DoE supported project.

1) We developed a high-fidelity computational model of a DC microdischarge that simulates the effect of physical transient phenomena in these discharges.
2) The model was used to simulate the effect of controllable electron injection on the microdischarge structure, specifically the role of discharge non-linearities and the dynamics of discharge structure modification in response to electron injection was simulated.
3) We demonstrate the effect of higher harmonic generation by exciting the microdischarge with a microwave signal. This has potential application for use of microdischarges as sources of very high-frequency microwave.
4) We have developed a Particle-In-Cell model for microdischarges driven by microwave excitation. Several aspects of microwave excitation have been elucidated.

Personnel supported as part of project:

The following individual were supported as part of the project:

1) Laxminarayan Raja (PI)
2) Premkumar Paneelchelvam (Graduate Research Assistant)
3) Dmytro Levko (postdoc)

Presentations and Publications resulting from this work:

The following conference presentations (talk/poster) and journal publications resulted from this work.

Conference talks and proceedings:

1) P. Paneerchelvam and L. L. Raja "Computational Modeling of plasma control using electron injection from surfaces", Gaseous Electronics Conference (GEC 2014) (Poster)
2) P. Paneerchelvam and L. L. Raja "Computational modeling of electron injection in a DC microdischarge", 8th International Workshop on Microplasmas (IWM 2015) (Poster)
3) L. L. Raja, "Simulation of atmospheric pressure cold plasma jets and their interactions with surfaces," 8th International Workshop on Microplasmas, Newark, NJ, USA, 11-14th May 2015. (Invited Talk)
4) P. Paneerchelvam and L. L. Raja "Harmonic generation in microwave microdischarges", Gaseous Electronics Conference (GEC 2015) (Talk)

Journal Publications:

1) Premkumar PanneerChelvam and Laxminarayan L. Raja**, "**Computational Modeling of the effect of external electron injection into a direct-current microdischarge", *Journal of Applied Physics*, **118**, 243301 (2015)
2) D. Levko and L. L. Raja, "Effect of frequency on microplasmas driven by microwave excitation," *Journal of Applied Physics*, Vol. 118, 2015, pp. 043303.
3) D. Levko and L. L. Raja "Electron kinetics in atmospheric-pressure argon and nitrogen microwave microdischarge," (submitted).
4) D. Levko and L. L. Raja, "Influence of field emission on microwave microdischarges," *Journal of High Voltage Engineering* (submitted).

Following is a brief report of technical work done as part of this project:

Introduction

This is a colloborative research from The University of Texas at Austin (PI: Prof. Raja) and the University of Texas at Dallas (PI: Prof. Overzet). The objective of this work was to study the active control of plasma discharges. Prof. Overzet's group at UT Dallas worked on experiments for this work and our group at UT Austin worked on the computational modeling.

Secondary electron emission (SEE) from cathode surface is the key process that determines the overall discharge properties of a DC microdischarge operating in gamma mode. SEE is however a surface property that depends on the surface material and the nature of plasma species incident on the surface. No direct control of the electron emission by this mechanism is possible. In recent work, Eden and co-workers studied low-voltage controllable electron emitter devices embedded devices on the surface of a microdischarge cavity [1]. They demonstrated the ability to actively modulate light emission from microdischarges through the control of electron injection in these discharges.

Plasma discharge model:

A self consistent, multi-species, multi-temperature fluid model of plasma with finite rate chemistry is developed and used in this work. The governing equations of the model are as follows:

Governing Equations:

1) Continuity equation is solved for the number density of constituent species and is given as

$$\frac{\partial n_k}{\partial t} + \vec{\nabla}.\vec{\Gamma}_k = \dot{G}_k \qquad (Eq.1)$$

Here n_k is the number density of the species, $\vec{\Gamma}_k$ is the particle flux and $\dot{G}_k$ is the net rate of production of species. This equation is solved for all the species except for the dominant background gas. The number density of the background gas is obtained is calculated using the Ideal gas law. The particle flux $\vec{\Gamma}_k$ is calculated using the drift diffusion approximation.

2) Electron energy equation is solved for calculating the electron temperature and is given by

$$\frac{\partial}{\partial t}\left(\frac{3}{2}k_B n_e T_e\right) + \vec{\nabla}.\left(\frac{5}{2}k_B T_e \overrightarrow{\Gamma_e} - \kappa_e \vec{\nabla} T_e\right)$$

$$= e\overrightarrow{\Gamma_e}.\overrightarrow{\nabla}\phi - \frac{3}{2}k_B n_e \frac{2m_e}{m_{k_b}}(T_e - T_g)\bar{\nu}_{e,k_b} - e\sum_{j=1}^{I_g}\Delta E_j r_j \qquad (Eq.2)$$

Here, κ_e is the thermal conductivity of electrons, $\overrightarrow{\Gamma_e}$ is the electron particle flux, m_e and m_{k_b} are the molecular mass of electron and the dominant background species respectively, $\bar{\upsilon}_{e,k_b}$ is the electron momentum transfer collision frequency with the background species, ΔE_j is the energy lost per electron (in eV) in an inelastic collision represented by a gas phase reaction j, r_j is the rate of the progress of the reaction j. The first term in the right hand side of the above equation is the electron Joule heating term. The second term is the energy lost due to elastic collision and the third term is the energy lost due to inelastic electron impact reactions.

3) Gas energy equation is solved for calculating the gas temperature and is given by

$$\frac{\partial}{\partial t}\left(\sum_h \frac{f_k}{2}k_B n_k T_g\right) + \vec{\nabla}.\left(\sum_h\left(1 + \frac{f_k}{2}\right)\frac{5}{2}k_B T_e \overrightarrow{\Gamma_e} - \sum_h \kappa_h \vec{\nabla} T_g\right)$$

$$= -\alpha\left(e\sum_h Z_k \overrightarrow{\Gamma_k}\right).\overrightarrow{\nabla}\phi + \frac{3}{2}k_B n_e \frac{2m_e}{m_{k_b}}(T_e - T_g)\bar{\nu}_{e,k_b}$$

$$- e\sum_{j=1}^{I_g}\Delta E_j r_j \ . \qquad (Eq.3)$$

Here T_g is the common temperature of all the heavy species including ions, meta-stables and the dominant background gas. The common temperature assumption is valid because the energy transfer mean free path for the ions and the meta-stables is usually much lower than the discharge dimensions for typical microdischarges and classical large volume discharges.

4) The self-consistent electrostatic potential is obtained by solving the Gauss's law

$$\nabla^2\phi = -\frac{e}{\epsilon_0}\sum_k Z_k n_K \qquad (Eq.4)$$

Species transport:

The transport coefficients of the electrons are calculated using the local mean energy approximation, meaning, the electron transport coefficients are parameterized by the average electron energy. These coefficients are obtained by a zero-dimensional electron Boltzmann solver with the two term approximation and suitable averaging over the electron energy distribution functions using the open source software BOLSIG+ [2]. The heavy species transport coefficients are obtained using experimental data.

Plasma Chemistry:

Pure argon is considered as the working gas and the discharge pressure is 100 Torr. The finite-rate plasma chemical kinetics for high-pressure argon includes electrons (e^-), monomer and dimer positive ions (Ar^+, Ar_2^+), monomer and dimer metastable species (Ar^m, Ar_2^m), and neutral gas (Ar). The chemistry mechanism consists of electron impact ionization, excitation reaction, Penning ionization and three-body recombination reactions.

Simulation of active electron injection in microdischarge:

A metal-insulator-metal configuration with planar anode and cathode is used for this study. The cathode is assumed to be the source of active electron injection into the plasma. The insulator (dielectric) layer sandwiched between the electrodes consists of a hole of diameter 500μm and its thickness which is also equal to the inter electrode distance is 120μm. The schematic of the discharge configuration and the computational mesh used for this work is shown below Two probe points are considered in the plasma sub-domain to investigate the transient behavior of the discharge. Point A is near the edge of the cathode sheath at (r = 230μm, z = 20μm) with respect to the origin located at the intersection of the axis and the cathode surface. Point B is located at (r = 50μm, z = 100μm) in the bulk of the plasma.

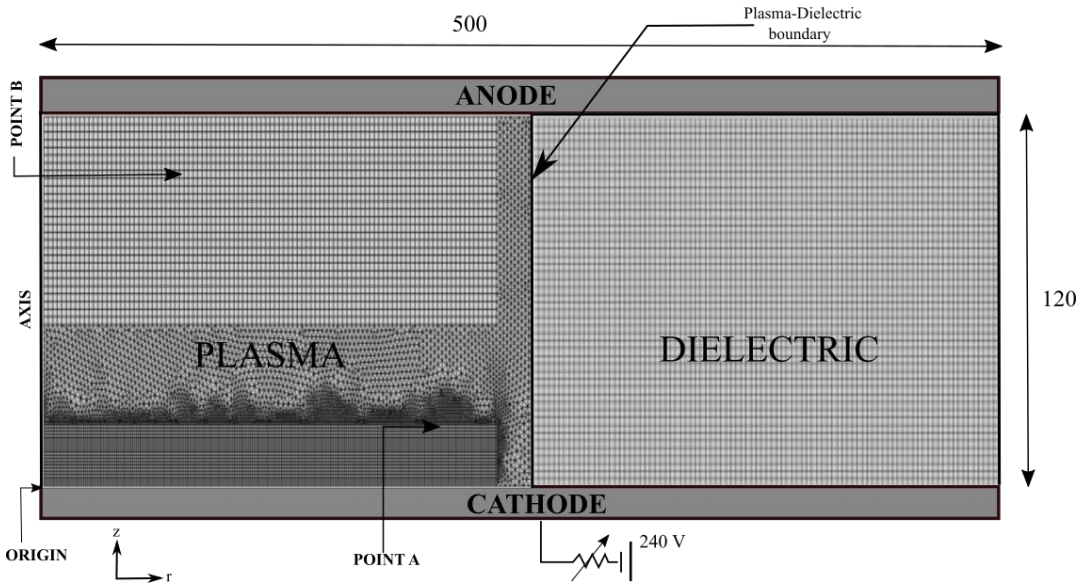

Figure 1: Schematic of microdischarge geometry and computational domain (All dimensions in μm).

Simulations are performed in two steps. The first is the simulation of steady microdischarge without active electron injection. Here, the discharge is sustained by the intrinsic secondary electron emission from the cathode surface. The secondary electron emission yield is assumed to be a constant value of 0.03 from both the cathode and anode. In the second step, electron injection from the cathode surface is activated in the pre-established steady discharge. The simulation is run in a time-accurate manner to fully resolve the dynamics of discharge transitions from a steady discharge sustained by the secondary electron emission mechanism to the discharge state with actively controlled electron injection.

Results and discussion:

The following figures compare the important microdischarge plasma parameters at the steady states before external injection, i.e. discharge sustained by secondary electron emissions only, and after electron injection. Fig 2 shows the variation of electrostatic potential in the plasma and dielectric subdomains. The sheath thickness decreases after electron injection owing to the increase in plasma density. Consequently the magnitude of electric field in the sheath after injection increases to almost twice the value before injection.

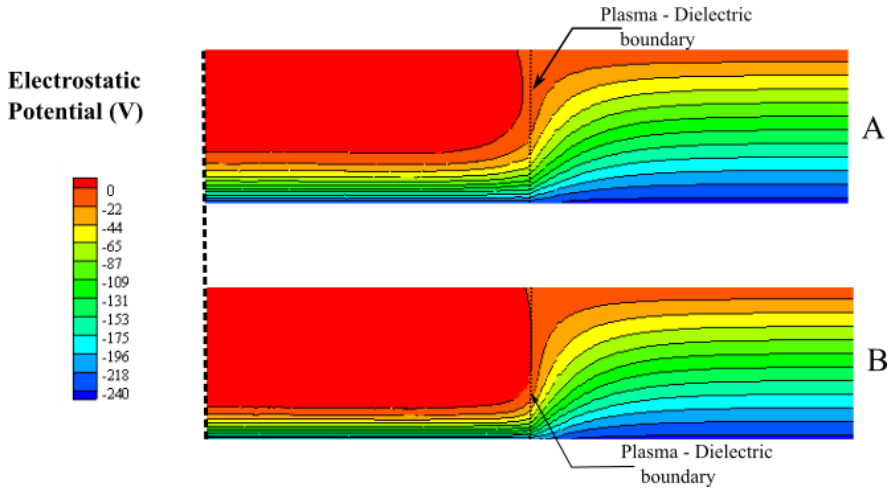

Figure 2: Steady state electrostatic potential (V) in the microdischarge before injection (A) and after injection (B). The region to right of the plasma-dielectric boundary is the dielectric.

Figure 3 shows the electron and monomer (dominant) ion (Ar^+) number density in the plasma. The number densities of e^- increases significantly by a factor of almost 5 after injection compared to before injection. The injected electrons from the cathode surface get energized in the sheath, where electric fields are high (of the order of 10^7 V/m), and in turn increase the rate of the electron impact ionization reaction (principally reaction G2 in Table 1) resulting in a rise in the volumetric production of electrons.

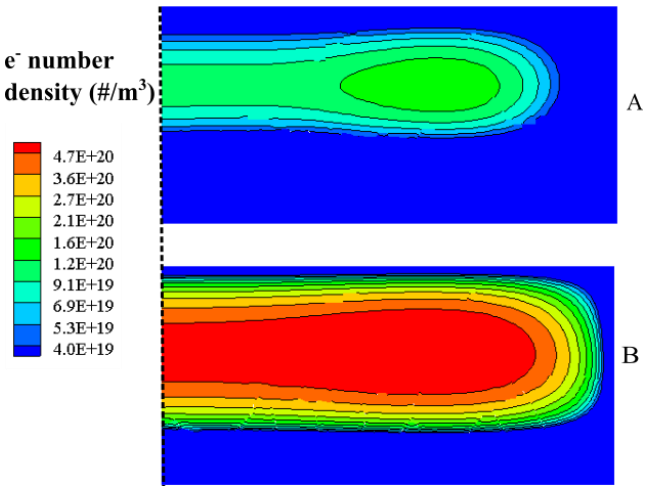

Figure 3: Steady-state electron density (#/m^3) in the microdischarge before injection (A) and after injection (B).

Figure 4 shows electron temperature in the plasma. The electron temperatures is a few eV in the bulk plasma and increases sharply to about 18 eV in the cathode sheath edge region for the case without electron injection. However, for the case with active electron injection, the electron temperature increases to over 25 eV in the cathode sheath edge, but remains unchanged in the bulk plasma.

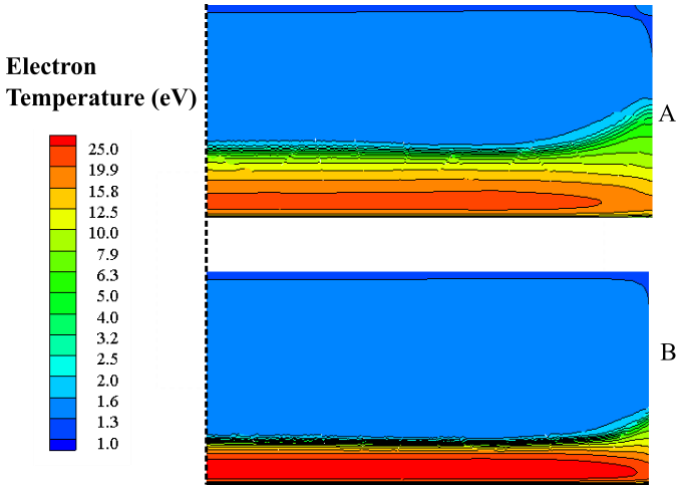

Figure 4: Steady state electron temperature (eV) in the microdischarge before injection (A) and after injection (B).

Figure 5 shows the change in conduction current at the anode (ΔI_c) (i.e. increase in the conduction current from steady state value before injection to a new steady state value after injection) as a function of increasing injected electron current at the cathode. For the baseline case without injection the steady state current measured at the anode 1.33 mA. As seen in the figure, ΔI_c is 2.33 mA for the injected current of 0.028 mA and increases to about 22 mA for an injected electron current of 2 mA. Over the range of injected electron currents studied, the anode current increases by nearly a factor of 10 indicating the strong non-linear coupling within the discharge. The non-linear amplification of the injected electron current is principally attributable to the non-linear mechanisms associated with the cathode sheath and plasma chemical reactions.

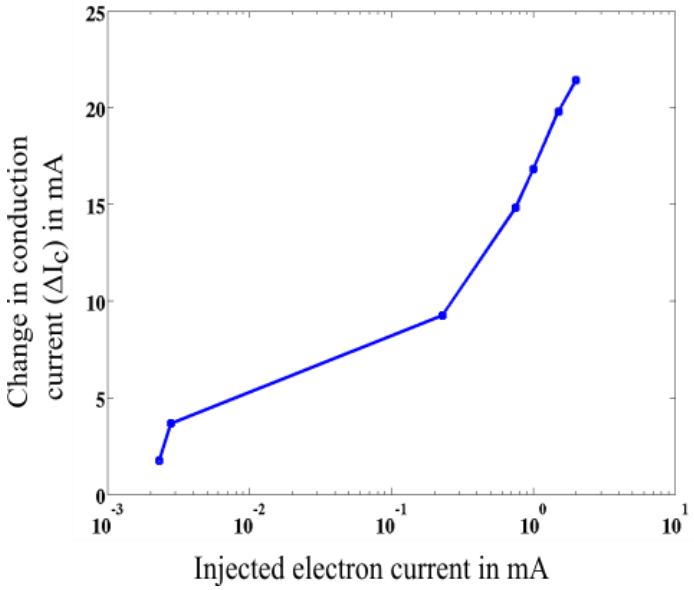

Figure 5: Variation of ΔI_c with injected electron current.

Solid state device model:

We have also developed a computational tool for the continuum description of the transport of charge carriers in a solid state material. The model solves the continuity equation (Eq. 1) for the charge carriers (electrons and holes) and Poisson's equation (Eq. 4) for the electrostatic potential. The computational model was validated using the transport of charge carriers in a one dimensional PN junction diode. A PN junction can be thought as bringing together a P-type and an N type semiconductor. Upon joining the two regions, electrons and holes diffuse across the junction resulting in diffusion current. However this diffusion cannot build indefinitely because of an electrostatic barrier created near the junction which results in an opposing electric field. This region of non-zero electric field is called the depletion region. When the junction is forward biased, the electrostatic potential barrier in the junction reduces and the opposite effect occurs for reverse bias.

The steady state result obtained by the model is reported here. The electrostatic potential profile predicted by the model is presented in figure 6. As can be seen there is a depletion region near the junction and the potential barrier reduces in the case of forward bias and increases in the case of reverse bias when compared to equilibrium.

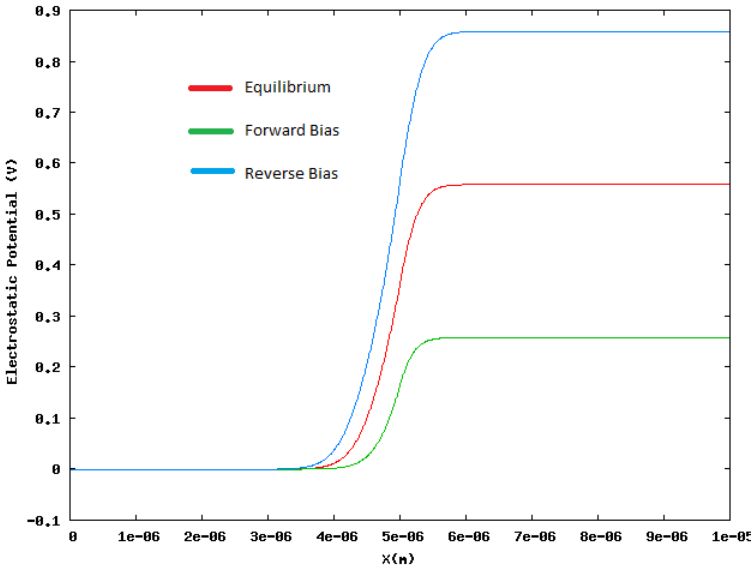

Figure 6: Variation of Electrostatic potential along the length of the diode

The number density of electrons is presented in figure 7 and the electric field is shown in figure 8. The model predicts a drop in the concentration of minority carriers near the edge of the junction. This is because the electric field in the depletion region for a reverse biased junction is very high that it sweeps the minority carriers up the potential barrier. The electric field is non-zero only in the depletion region and its strength reduces if forward biased and increases if reverse biased when compared to the equilibrium case.

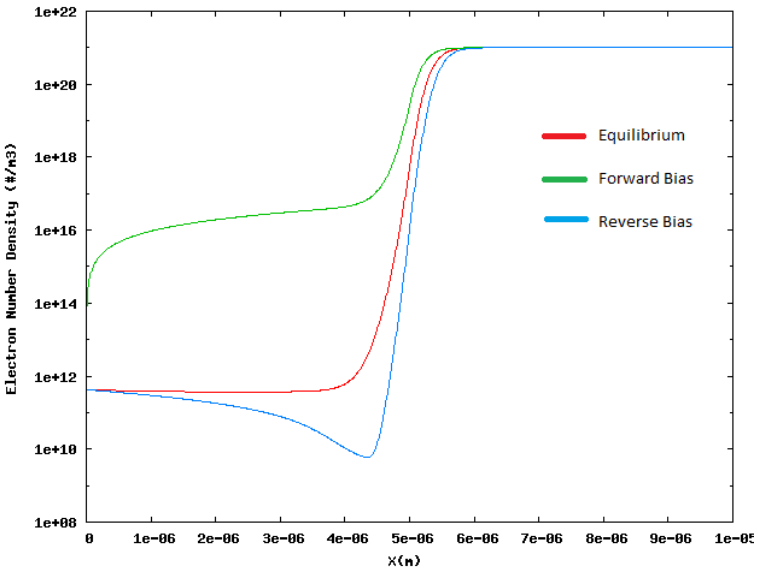

Figure 7: Number densities of electrons for various bias

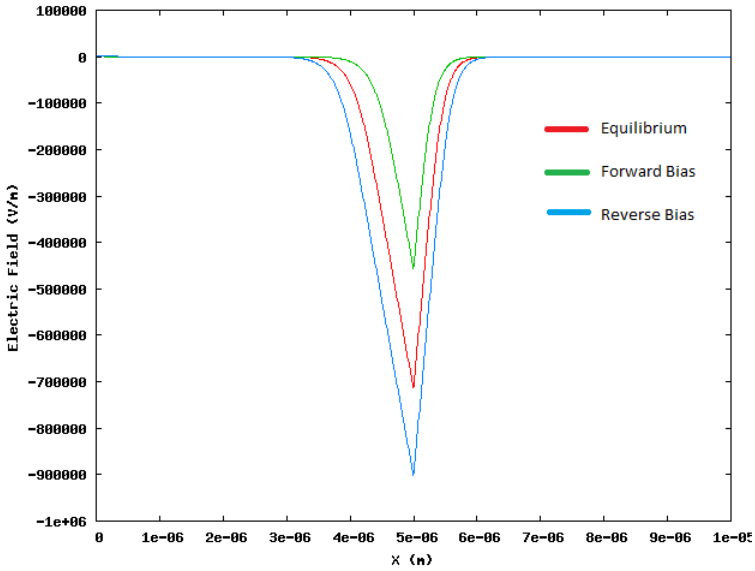

Figure 8: Electric field in the diode for various bias.

Simulation of microwave microdischarges:

As a part of this work, we also simulated microwave microdischarges using our Plasma discharge model. We particularly looked at the production of higher harmonics by these discharges. Microwave microdischarges are plasma discharges that are created using a AC source whose frequency is in the microwave regime (0.3 - 10 GHz). These discharges are sustained in high pressures (100 Torr – 1 atm). The number density of electrons in these discharges are of the order of 10^{20} #/m^3. These are non-equilibrium plasmas with high electron temperature of the order of 1 eV. The heavy species temperature is typically of the order 300 – 1000K.

We simulated a microwave microdischarge in a 1 dimensional geometry. The number of cells in the plasma domain is 1000. The working gas in the plasma is Argon and the pressure in the discharge is assumed to 100 Torr. We considered a planar geometry and the inter-electrode gap is set to be 100 μm. The secondary electron emission from both the electrodes is fixed to 0.2.

We looked at source voltages of 75 V and 50V and frequencies of 2, 4 and 10 GHz. The

electron number density and electron temperature sustained in discharge as it reaches quasi steady state for varying source voltage and frequency is plotted in figure 9. For the 75V/2GHz source, the peak electron density obtained was about 3 x 10^{20} #/m^3 and the electron temperature in the bulk of the plasma was around 3 eV and in the sheath was around 10 eV. We can notice the sheath oscillating between the left and the right electrodes as the voltage changes periodically. For the 75V/4GHz source, the peak electron density is 9 x 10^{20} #/m^3 and the electron temperature in the bulk is around 3 eV and in the sheath around 11 eV. For the 50V/2GHz source, the peak electron density is 4.5 x 10^{21} #/m^3 and the electron temperature in the bulk and sheath were 3 eV and 11 eV respectively. It is evident that for a fixed voltage, as we increase the source frequency, we see a corresponding increase in the peak electron density and an increase in the electron temperatures in the sheath region.

We also studies the harmonic content of the current drawn by these discharges. Figure 10 shows the FFT results of the discharge current for the 75V/2 GHz source. It can be seen that the discharge produces up to 6^{th} harmonics with considerable strength. This suggests that microwave microdischarges are efficient sources for producing higher harmonic content of the source frequency. The reason for these harmonics are produced is the presence of strong non-linearities present in electron motion. It must be noted that discharge current is mainly dominated by the conduction current of the electrons. The electron motion is governed by a non-linear function of the driving fields and electron velocity in turn is non-linearly related to the electron current. As result of this functional dependence on electron motion on the conduction current we see strong harmonics produced by this discharge.

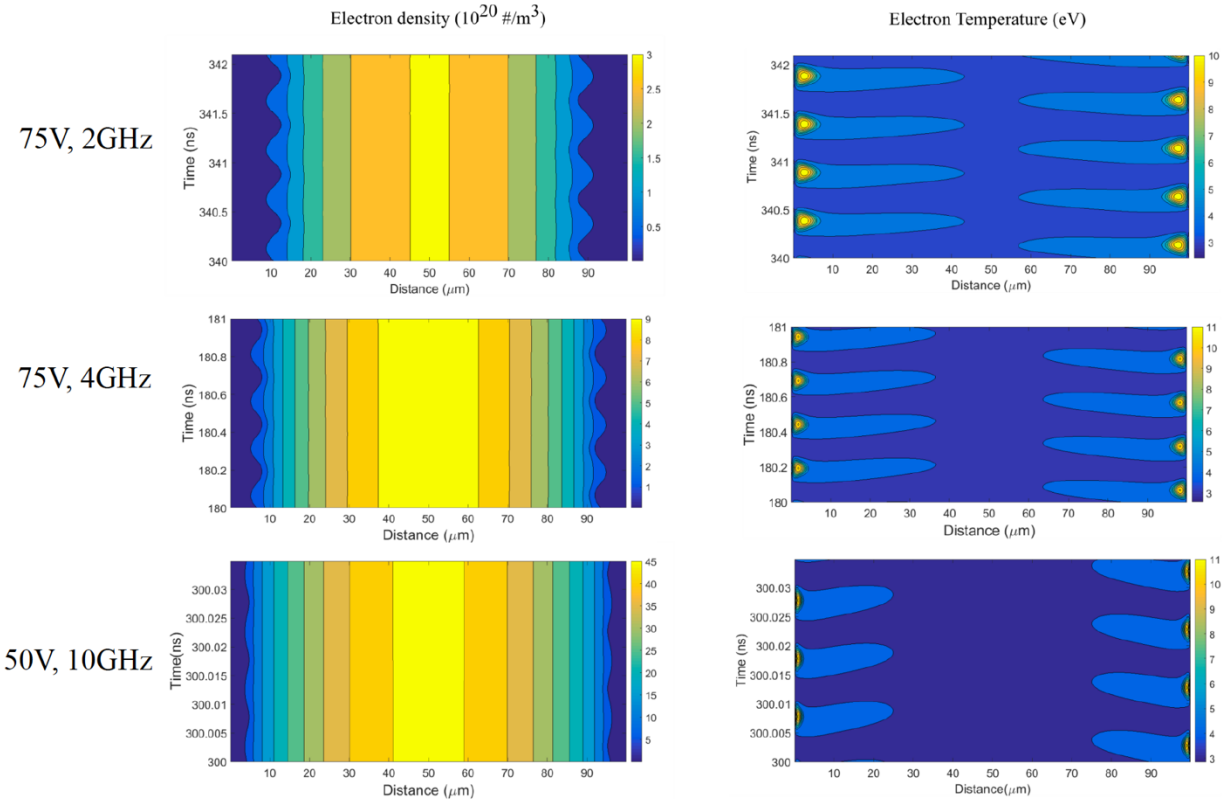

Figure 9: Electron Density and Electron temperature profiles for various voltage and frequency.

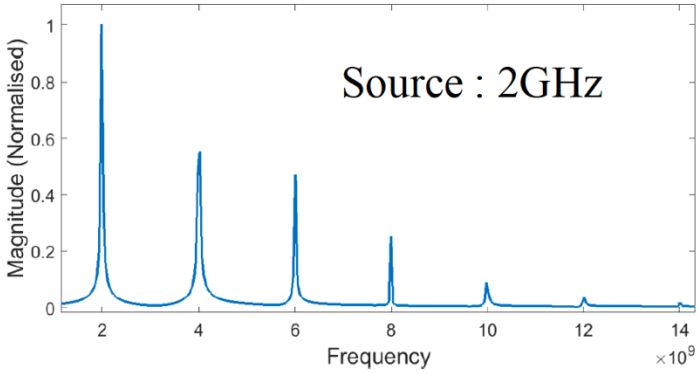

Figure 10: Fourier transform the discharge current

References:

[1] K.F. Chen, and J.G. Eden, "The plasma transistor: A microcavity plasma device coupled with low voltage, controllable electron emitter", *Applied Physics letters*, **93**, 161501 (2008).

[2] G.J.M. Hagelaar, L.C. Pitchford, "Solving the Boltzmann equation to obtain electron transport coefficients and rate coefficients", *Plasma Sources Sci. Technol.*", **14**, 722 (2005).